Dmitrii Burovikhin*, Panagiota Kitsopoulos, Michael Lauxmann, and Karl Grosh

Placement and Orientation of an Accelerometer Sensor Attached to the Human Incus in Hearing Implants

https://doi.org/10.1515/cdbme-2024-2033

Abstract: In this study a method for determining the best placement and optimal orientation of the implantable piezoelectric accelerometer attached to the short process of the incus is developed. The accelerometer is intended to be used as a replacement for an external microphone to enable totally implantable cochlea implants or as part of a totally implantable hearing aid. The best location is determined to be near the incudomalleolar joint. The optimal orientation of the sensor at the determined location is obtained using two criteria – maximum voltage sum and minimum loudness level sum. The method described in the paper can be used to further optimize the design and the performance of the accelerometer.

Keywords: accelerometer sensor, middle ear, incus, finite element method, cochlea implants

1 Introduction

Hearing aids (HAs) and cochlear implants (CIs) are among the primary solutions for permanent sensorineural hearing loss [1] and can improve speech perception and quality of life. In spite of their benefits, the adoption rates of both types of devices suffer from perceived ineffectiveness, ongoing maintenance costs, lack of comfort, activity limits, and aesthetics [2,3]. A totally implantable auditory prosthesis (TIAP) that would require surgical implantation of all device components (including a sensor to replace the current external commercial microphones used in HAs and CIs) can address some of these issues.

In literature, there are various examples of prototype implantable sensors, with some detecting the acoustic vibrations directly (e.g., implantable microphone [4,5]), some detecting the resulting vibrations of the middle ear bones/eardrum (e.g., accelerometer [6,7,8]), and some detecting the pressure changes within the inner ear (e.g., pressure sensor [9]). However, there is presently no available implantable sensor that is able to adequately meet the performance (operational frequency bandwidth, 100 Hz - 8 kHz) that rivals commercial microphones and specifications (low noise and small size) for the intended prosthetic application; this gap motivates our research. We note that there is one study on a totally implantable cochlear implant [10]; however, this device seems to have had low adoption and the subcutaneous microphone used in the device suffered from reduced acoustic performance. The work in this paper is based on the piezoelectric accelerometer proposed in [11], which has the potential to meet the required space constraints and the 20-phon noise floor over the 100 Hz - 8 kHz frequency range.

The paper presents a method for determining the best placement of the piezoelectric accelerometer on the short process of the incus as well as its optimal orientation at that location. The investigation is conducted with the help of a finite element (FE) middle-ear model developed by [12] and adapted by [13]. The FE model is used to simulate the rigid body motion of the ossicles. Based on the simulated rigid body motion of the incus and the sensor's sensitivity curves derived from an analytical model the voltage output of the accelerometer is determined and optimized with the help of a MATLAB script to find its best placement and orientation.

2 Materials and Methods

2.1 Accelerometer Design and Sensitivity

The accelerometer design from [11] is shown in Figure 1. It consists of two proof-mass-loaded piezoelectric cantilever bimorph plates also called sensing elements – low frequency sensing element (LFSE) and high frequency sensing element (HFSE) - made of aluminium nitride (AlN) and capable of converting mechanical vibrations to electrical signals (voltage output). The plane-strain constitutive hypothesis is assumed. The sensor design also includes a silicone frame surrounding the sensing elements and a titanium lid, which is not shown. The entire device is placed on a printed circuit board (PCB)

***Corresponding author: Dmitrii Burovikhin:** Reutlingen University, Reutlingen, Germany, e-mail: dmitrii.burovikhin@reutlingen-university.de
2nd Author Panagiota Kitsopoulos: University of Michigan, Ann Arbor, USA
3rd Author Michael Lauxmann: Reutlingen University, Reutlingen, Germany
4th Author Karl Grosh: University of Michigan, Ann Arbor, USA

that includes the signal processing electronics and filtering to extract the voltage output from each sensing element.

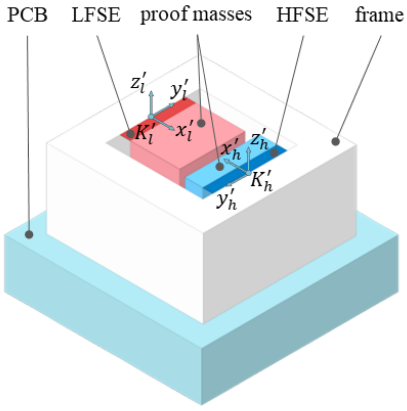

Figure 1: Design of the accelerometer.

Each sensing element is responsible for a specific frequency bandwidth. The LFSE operates in the range from 100 Hz to 1.25 kHz, whereas the HFSE operates above 1.25 kHz. When the sensor is subjected to a displacement excitation, the sensing elements deform and produce voltage due to their piezoelectric properties. The silicone proof masses sit flush against the sensing elements and help adjust their natural frequencies.

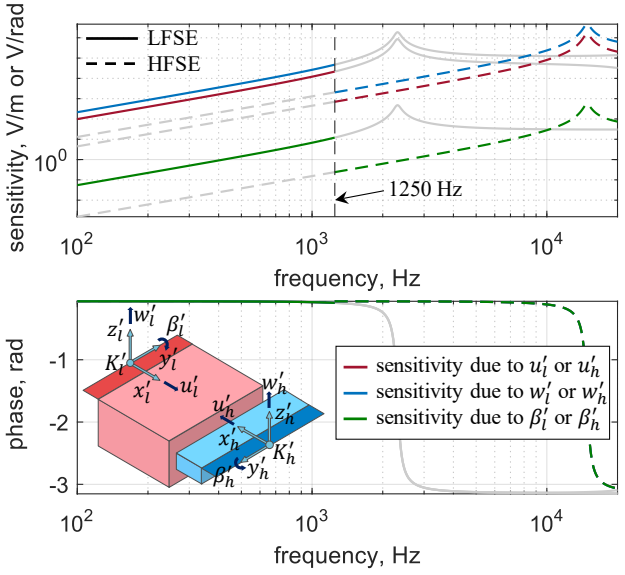

Figure 2: The sensitivity curves of each sensing element. The greyed-out sections in each graph represent the sensing elements' cease of operation outside their frequency bandwidths. u_l', v_l', w_l', α_l', β_l', and γ_l' are the elemental displacement excitations corresponding to the LFSE; u_h', v_h', w_h', α_h', β_h', and γ_h' are the elemental displacement excitations corresponding to the HFSE.

The analytical model of the sensor presented in [11], [15] and [16] is used to derive the sensor's sensitivity curves shown in Figure 2. The sensitivity is defined as each sensing element's voltage output normalized to the subjected elemental displacement excitation (V/m). Since the sensing elements are far more sensitive to the transversal excitation along the x- and z-axes and to the rotational excitation around the y-axis of the corresponding coordinate systems K_l' and K_h' (u_l', w_l', β_l' and u_h', w_h', β_h'), the other three degrees of freedom (v_l', α_l', γ_l' and v_h', α_h', γ_h') are neglected.

2.2 Middle-Ear Finite Element Model

The FE middle-ear model used for this study is developed in ANSYS 2024R1 and shown in Figure 3. The current model is based on the model developed in Hypermesh (Altair Engineering, Inc.) by [12] with a few changes. A longer 40 mm ear canal is introduced, as well as a closed tympanic cavity. All the parameters and material properties are adopted from the Hypermesh model. The geometry of the tympanic membrane (TM), the ossicles, the ear canal, and the tympanic cavity are reconstructed using micro-CT.

2.3 Placement and Anatomical Restrictions

Even though placing the sensor on the malleus may lead to a better sensor performance as the umbo can achieve higher accelerations [14], the surgical risks that come with accessing the umbo through the facial recess (facial nerve) make the malleus a less desirable attachment point. However, the short process of the incus does not require the facial recess approach and can be accessed through only a mastoidectomy. Thus, the short process of the incus is a location worth investigating in more detail which is the primary goal of this study.

2.4 Optimal Position for the Accelerometer

Figure 3(a) shows the initial search space for the optimal placement of the sensor. The colour code shows that the highest voltage output is reached near the incudomalleolar joint. As the result of this preliminary investigation several sample points are chosen along the incus surface and around it as shown in Figure 3(b).

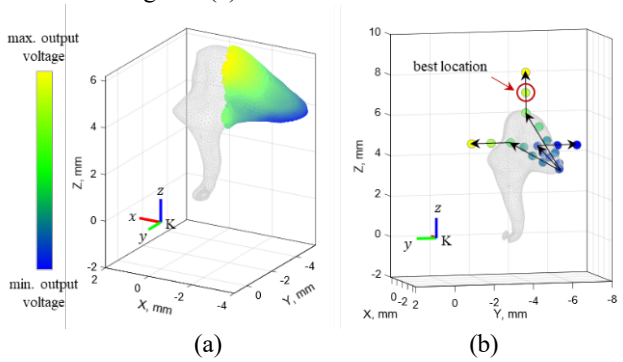

Figure 3: (a) The search space according to max. voltage sum criteria (the locations with higher voltage values are color-

coded yellow and with the lower ones - blue); (b) the sample points selected around the short process of the incus.

The rigid body motion at the centre of mass of the incus is derived from the FE model under the harmonic pressure load at the inlet of the ear canal of 1 Pa (94 dB SPL) in the global coordinate system K located at the centre of the stapes footplate, see Figure 4. Assuming that the accelerometer is rigidly attached to the incus, the translational and rotational displacements at any given point on the accelerometer can be derived from the rigid body motion of the incus.

The voltage output (V/Pa) produced by each sensing element is calculated by multiplying each element's displacement vector ($\boldsymbol{u}_l'$ and $\boldsymbol{u}_h'$) with the corresponding sensitivity curves and summing up the resulting voltage components.

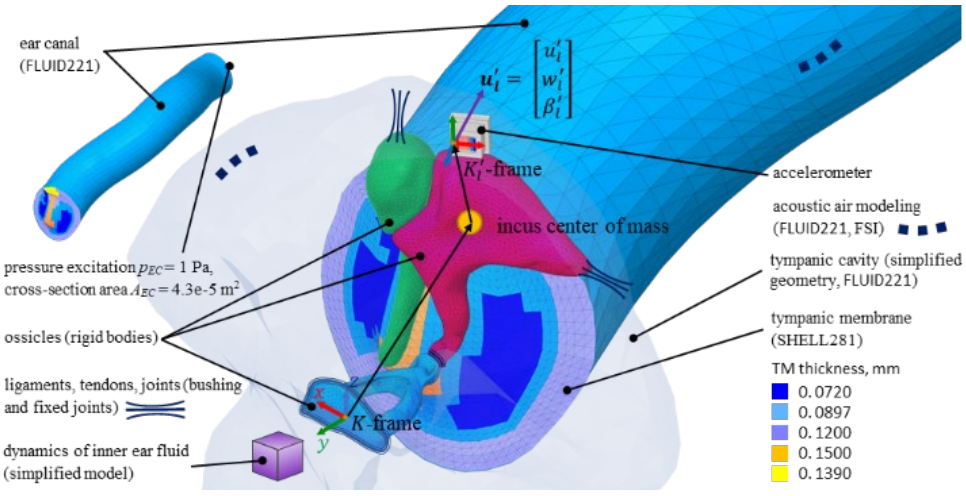

Figure 4: The finite element model of the middle ear with the accelerometer. $\boldsymbol{u}_l'$ is the displacement vector of the LFSE in the K_l'-frame. K_h'-frame is not shown.

To evaluate the results, the maximum voltage sum and the minimum equivalent loudness level sum criteria are used. For the first criterion, the goal is to maximize the sum of two voltage outputs by altering the accelerometer's placement and orientation until the maximum value is reached. The first voltage output is produced by the LFSE at 500 Hz and the second is produced by the HFSE at 7 kHz. For the second criterion, the goal is to minimize the sum of the equivalent loudness level values. The first value is produced by the LFSE at 500 Hz and the second is produced by the HFSE at 7 kHz. The equivalent loudness level values of pure tone frequencies are measured in phon and are calculated from the noise equivalent sound pressure level in accordance with [17].

3 Results

Figure 3(b) shows that the accelerations are higher at the points that are farther away from the centre of mass of the incus. However, the wall of the tympanic cavity poses an anatomical restriction, so that the sensor cannot be placed too far away from the incus. On the other hand, the accelerometer will be attached to the short process of the incus via a clip which is expected to add a short distance of at least 1 mm between the accelerometer and the surface of the incus. Taking that into account and considering all the anatomical and surgical restrictions, the point near the incudomalleolar joint, located at a distance of about 1 mm from the bone's surface in the superior direction (the global z direction) is chosen as the best placement point, see Figure 3(b).

The determined optimal placement and orientation for the accelerometer based on the two criteria is shown in Figure 5. For each of the two criteria, three different views are shown relating the global coordinate system, K, to the accelerometer's coordinate system K′.

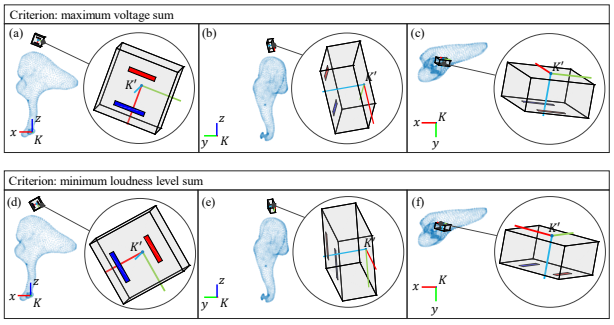

Figure 5: (a),(b),(c) views of the optimal orientation of the accelerometer found through the maximum voltage criterion; (d),(e),(f) views of the optimal orientation of the accelerometer found through the minimum loudness level criterion.

In addition, Figure 6 shows the equivalent loudness curves to compare the results for both criteria.

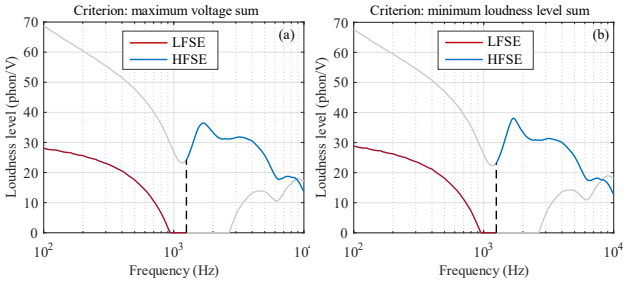

Figure 6: Loudness level for the two criteria a) and b).

4 Discussion

As Figure 6 shows, both criteria yield similar total voltage output results. However, the maximum voltage sum criterion gravitates to finding the best orientation for the LFSE at the expense of the HFSE. This occurs because the LFSE produces a much higher voltage at 500 Hz than the HFSE at 7 kHz. Thus, the LFSE has a larger contribution to the sum than the HFSE, and as the algorithm maximizes the sum, it favours the LFSE. In contrast, the minimum equal loudness sum criterion tends to favour the HFSE as it produces a lower equal loudness value at 7 kHz than the LFSE at 500 Hz, and the algorithm searches for the minimum sum.

Both criteria result in the accelerometer's y-axis (K'-frame) pointing in the same direction as the global y-axis (K-frame), while the accelerometer's y-axis points along the short process of the incus. In general, the voltage produced by the sensing elements in response to the translational excitation along the z- axis (K′-frame) is the largest contributor to the overall output voltage. Considering that the incus naturally performs a rocking motion around the global x-axis (K-frame), it makes sense that the accelerometer's z-axis (K′-frame) points in the same direction as the global y-axis (K-frame).

Lastly, there are two main aspects of this study that have not been fully investigated. One is the influence of the accelerometer's mass on the overall dynamics of the system. The other is the connection of the accelerometer to the incus. In reality, this attachment will utilize a clip with a certain elasticity. The more compliant this connection is, the more effect the accelerometer's mass will have on the system's performance.

5 Conclusion

In this study, a comprehensive optimization approach was used to determine the location and orientation of a middle ear accelerometer for use as a part of a completely implantable auditory prosthesis. The optimal configuration of the piezoelectric accelerometer attached to the short process of the incus was found to be near the incudomalleolar joint 1 mm away from the surface of the incus in the superior direction with the z-axis of the accelerometer pointing towards the stapes' footplate and y-axis pointing along the short process of the incus towards its posterior ligament (see Fig. 5). While existing completely implantable cochlear implants have been developed in the past [10], they have not had wide adoption. A recent study concluded that the remaining technical barrier for wider adoption is the development of a low-noise, robust sensor [18]. We advocate here for an ossicular accelerometer, which inherits the protection of the middle ear along with the more naturalistic sound (e.g., pinna cues and ear canal dynamics).

Author Statement

Research funding: research reported in this publication was supported by the US National Institutes of Health under Award Number R01DC021596. The content is solely the responsibility of the authors and does not necessarily represent the official views of the National Institutes of Health. Conflict of interest: Authors state no conflict of interest. Informed consent: Informed consent has been obtained from all individuals included in this study. Ethical approval: the conducted research is not related to either human or animals use.

References

[1] Cunningham LL, Tucci DL. Hearing Loss in Adults. N Engl J Med; 2017; 377(25):2465–2473.

[2] Blazer DG, Domnitz S, Liverman CT, Committee on Accessible and Affordable Hearing Health Care for Adults; Board on Health Sciences Policy; Health and Medicine Division; Hearing Health Care for Adults: Priorities for Improving Access and Affordability. Washington (DC): National Academies Press (US); September 6, 2016.

[3] Calero D, Paul S, Gesing A, Alves F, Cordioli JA. A technical review and evaluation of implantable sensors for hearing devices. BioMedical Engineering OnLine; 2018; 17(1):23.

[4] Bruschini L, Forli F, Santoro A, Bruschini P, Berrettini S. Fully implantable otologics met carina device for the treatment of sensorineural hearing loss. preliminary surgical and clinical results. Acta Otorhinolaryngol Ital; 2009; 29(2):79–85.

[5] Pulcherio J, Bittencourt AG, Burke PR, Monsanto R, de Brito R, Tsuji R, Bento R. Carina® and esteem®: a systematic review of fully implantable hearing devices. PLoS One; 2014; 9(10), e110636.

[6] Sachse M, Hortschitz W, Stifter M, Steiner H, Sauter T. Design of an implantable seismic sensor placed on the ossicular chain, Medical Engineering & Physics; 2013; 35(10):1399–1405.

[7] Jia X, Gao N, Xu X, Wu Y, Kang H, Chi F. A new floating piezo-electric microphone for the implantable middle ear microphone in experimental studies; 2016; 136(12):1248–1254.

[8] Park W. Encapsulated Sub-millimeter Piezoresistive Accelerometers for Biomedical Applications. PhD thesis; 2006; Stanford University.

[9] Creighton F, Guan X, Park S, Kymissis I, Nakajima H, Olson E. An intracochlear pressure sensor as a microphone for a fully implantable cochlear implant. Otology & neurotology; 2016: 37.

[10] Briggs JS et al., Initial Clinical Experience With a Totally Implantable Cochlear Implant Research Device, Otology & Neurotology, 2008, 29:114Y119.

[11] Hake AE, Kitsopoulos P, Grosh K, Design of piezoelectric dual-bandwidth accelerometers for completely implantable auditory prostheses. IEEE Sensors Journal; 2023; 23(13):13957–13965.

[12] Sackmann B, Eberhard P, Lauxmann M, Parameter identification from normal and pathological middle ears using a tailored parameter identification algorithm. J Biomech Eng; 2021; 144(3): 031006.

[13] Burovikhin D, Dalhoff E, Wagner A., Schneider F, Lauxmann, M, Finite element model of a piezo-electric actuator coupled to the middle ear, 2023, J Biomech Eng, 145(2).

[14] Goode R, Ball G, Nishihara S, Nakamura K. Laser doppler vibrometer – a new clinical tool for the otologist. Am J Otol; 1996; 17(6):813–822.

[15] Hake AE, Zhao C, Sung W, Grosh K. Design and experimental assessment of low-noise piezoelectric microelectro-mechanical systems vibration sensors. IEEE Sensors Journal 21(16); 2021:17703–17711.

[16] Kitsopoulos P, Hake AE, Stucken EZ, Welch CM, Grosh K, Design and testing of ultraminiature MEMS middle ear accelerometers. AIP Conf. Proc. 27 Feb. 2024; 3062 (1): 040002.

[17] BS ISO 226:2003 (2003), Acoustics - Normal equal-loudness-level contours.

[18] Trudel M. and Morris DP, The remaining obstacles for a totally implantable cochlear implant, Current opinion in otolaryngology & head and neck surgery 30(5), 298–30.